JOURNAL OF PHYSICAL CHEMISTRY, 2025, Vol. 99, No. 1, c. 45–61

CHEMICAL KINETICS AND CATALYSIS

KINETIC MODEL OF THE TEMPERATURE-PROGRAMMED DESORPTION OF AMMONIA TO STUDY THE ACIDITY OF HETEROGENEOUS CATALYSTS

A. I. Lysikov[a,b,*], V. A. Vdovichenko[a,b], E. E. Vorob'eva[a,b], I. A. Shamanaeva[a,b], E. V. Luzina[a,b], L. V. Piryutko[a], Zh. V. Veselovskaya[a,b], and E. V. Parkhomchuk[a,b]

[a] *Boreskov Institute of Catalysis SB RAS (IC SB RAS), Novosibirsk, 630090 Russia*

[b] *Novosibirsk State University (NSU), Novosibirsk, 630090 Russia*

**e-mail: lyanig@catalysis.ru*

Received February 04, 2024
RevisedJuly 02, 2024
Accepted July 17, 2024

Abstract. A new method for processing the results of the temperature-programmed desorption (TPD) of ammonia from heterogeneous catalyst surfaces and an approach for automatic deconvolution of TPD kinetic curves are proposed. This method uses the Polanyi-Wigner kinetic model with formal kinetics approaches for simple reactions, which imposes restrictions on the observed orders of 1, 2, or 3. The parameters of TPD curves are selected based on the inverse simulation using the Runge-Kutta method and fitting them to experimental points using dynamic model parameters changes. As an example, several heterogeneous catalysts are presented in this work. TPD-NH_3 of titanium silicalite-1 and silicalite-1 is obtained using one third-order desorption kinetic equation. TPD-NH_3 of the three samples of γ-alumina is obtained using two desorption peaks with similar kinetic parameters.

Keywords: *temperature-programmed desorption, kinetics, ammonia, acidity, heterogeneous catalysts, alumina, silicalite^{-1}, titanium silicalite^{-1}*

DOI: 10.31857/S00444537250105e9

INTRODUCTION

The study of catalysts in the process of temperature-programmed desorption (TPD) of ammonia is a standard method of physicochemical identification of acidic properties of the surface [1–3]. However, the process itself is most often reduced to the determination of integral acidity and the separation of acid centers by strength into weak, medium, and strong [4–6]. Such a description of the process is empirical and uninformative since it fails to explain the structure of ammonia adsorption and desorption centers and has no predictive character [7–9]. Moreover, comparison of acid centers of catalysts with this approach is possible only for samples studied on the same device under absolutely identical conditions. If any of the process parameters, such as the heating rate, is changed, the ammonia TPD patterns may change to a large extent.

In the field of heterogeneous catalysis, monitoring specific catalyst properties such as the number of acid, basic or metal centers can be of paramount importance for the development of catalyst compositions and preparation methods, which can significantly increase the yields and selectivities of the target products. In addition, a rigorous quantitative description of properties is fundamental to the development of the mathematical apparatus of materials science. Obtaining standardized data using the ammonia TPD method will allow comparing catalysts obtained by different groups of researchers, which is necessary, among other things, for control and optimization of industrial catalysts. Therefore, the development of kinetic models of the ammonia desorption process, is an urgent practical task [10].

To date, determination of the concentration of acid centers is the only rigorous application of this method [11, 12]. The presence of two or more overlapping peaks in ammonia desorption does not allow to separate them correctly since there is no single physical model for processing the integral curves, the deconvolution of the TPD curve into Gaussian peaks being used most commonly [13]. However, such an empirical method of processing experimental results in most cases lacks any physical sense [14]. The development of an analytical method for processing ammonia TPD curves will allow obtaining information both on the number of acid centers and on their strength and type, mobility of adsorbed ammonia molecules, which will be the next step in the evolution of the TPD theory [15, 16].

It is worth noting that a number of models for mathematical description of the results of temperature-programmed ammonia desorption have already been published, for instance in [17]. The approach proposed by the authors is based on pseudo-equilibrium processes of ammonia readsorption and is descriptive only for monocenter adsorption when it is possible to identify the maximum value of the desorption peak commonly used to estimate the enthalpy change of adsorption. Using such a readsorption approximation is not justified in some cases incorrectly.

The authors in [18] performed analytical deconvolution based on the desorption kinetics; however, the readsorption of ammonia was also considered for the studied aluminum oxide in the low-temperature region.

The authors in [18–20] propose to use the Polanyi-Wigner theory to describe the desorption kinetics

$$-\frac{d\theta_{NH_3}}{dT} = \frac{\nu}{\beta}\theta_{NH_3}^{n}\exp\left(-\frac{E_D}{RT}\right), \quad (1)$$

where θ is the degree of filling of acid centers of the surface, n is the observed reaction order, E_D is the desorption activation energy, ν is the free frequency of vibration of ammonia molecule on the catalyst surface, and $\beta = d\mathrm{T}/dt$ is the heating rate, which is most often a constant value in the TPD methodology. This model may be suitable for studying acidity of a range of catalysts, but the descriptive nature of the model has limitations due to the choice of observed orders, which classically vary in the range $n = 0, 1, 2$ [21].

TPD Theory

In their work, Simoní Da Ros et al. described desorption of ammonia on aluminum oxide using a kinetic model of reversible desorption based on a simple Langmuir model [18]

$$\frac{d\theta_{NH_3,i}}{dt} = k_{A,i}P_{NH_3}\left(1-\theta_{NH_3,i}\right) - k_{D,i}\theta_{NH_3,i}, \quad (2)$$

$$\frac{dC_{NH_3}}{dt} = \frac{-C_{NH_3}}{\tau} + \frac{1-\varepsilon}{\varepsilon}\rho_p\left(-\sum_{i=1}^{NS}N_i\frac{d\theta_{NH_3,i}}{dt}\right), \quad (3)$$

where $k_{A,i}$ is the adsorption rate constant, $k_{D,t}$ is the rate constant of ammonia desorption from the c-type of centers, $\theta_{NH3,t}$ and N_t are the degree of surface filling of the ith type of acid centers and their integral concentration, ρ is the bulk density of the sample, P_{NH3} is the current ammonia pressure, ε is the porosity, and $\frac{C_{NH_3}}{\tau}$ is the ammonia mass transfer rate from the reactor, which is neglected in the model due to small sample loading (~200–700 mg).

Note that for the first type of acid centers (low-temperature peaks) on aluminum oxide, the authors in [18] considered the kinetics taking into account the readsorption process. In that work, the experiment was carried out with a constant nitrogen supply of 19 mL/min, in the flow of which ammonia was registered at the reactor outlet. Data processing yielded the activation energies for adsorption 73.05 kJ/mol and desorption 113.1 kJ/mol, pre-exponential adsorption multipliers 0.0488 $atm^{-1}min^{-1}$ and desorption 88.23 min^{-1} with total concentration of adsorption centers 0.696 mmol/g (for the bulk density of the aluminum oxide sample 0.96 g/cm^3) were presented for the low-temperature peak. Using these data of the time dependence of the concentration of released ammonia, the temperature dependences of adsorption and desorption rate constants, the integral acidity and bulk density of the catalyst, one can estimate the values of equilibrium constants, the degree of surface filling and, as a result, the dependence $\Delta_r G(T)$ for desorption from these centers in the temperature range 150–600°C.

The result of this estimation is shown in Fig. 1 (see Supplementary Materials for details). One knows that if the change in the Gibbs potential of the process is less than zero by more than 3 RT [22], the reaction proceeds practically irreversibly, i.e., in this case the assumption on equilibrium desorption and, consequently, readsorption of ammonia is incorrect. Note that the obtained values of standard enthalpy and entropy (40.03 kJ/mol and 62.36 J/(mol K), respectively) for the process of ammonia desorption in this work agree with the generally accepted values that were obtained in other works [20, 23].

The demonstrated irreversible character of desorption cannot be described correctly using a simple Langmuir adsorption-desorption scheme since the pressure of ammonia released during desorption is insufficient to approach the conditions of the equilibrium reaction.

For these reasons, we propose a kinetic model for irreversible ammonia desorption using the approach presented in [19]. According to the Polanyi-Wigner model, the kinetic equation of ammonia desorption can be written using Eq. (1) for each ith type of centers as the rate of decrease in the degree of surface filling with ammonia depending on the temperature and given the constant heating rate β

$$-\frac{d\theta_{NH_3,i}}{dT} = \frac{\nu_i}{\beta}\theta_{NH_3,i}^{n_i}\exp\left(-\frac{E_{D,i}}{RT}\right), \quad (4)$$

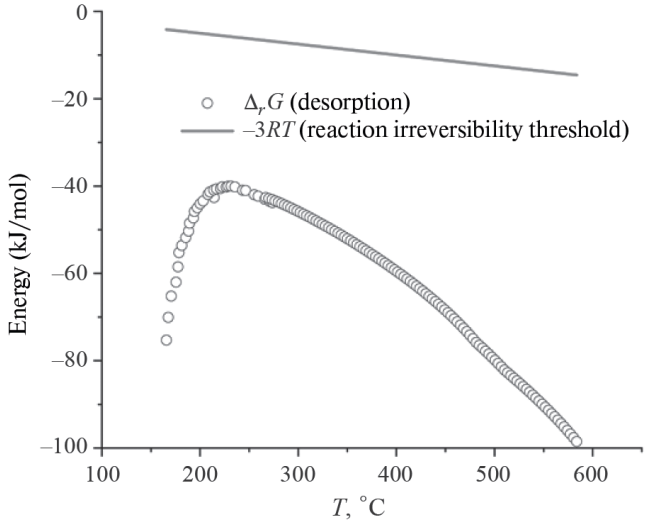

Fig. 1. Evaluation of the change in the Gibbs potential for the reversible desorption of ammonia from low-temperature aluminum oxide centers versus the reversibility threshold of the reaction – 3 *RT* [18].

this kinetic equation formally describes the chemical reaction on the catalyst surface through the activated state with participation of n_i adsorbed ammonia molecules in the form

$$n_i\theta_{NH_3,i} \overset{K^{\neq}}{\rightleftarrows} \left[NH_3 \cdots \theta_i \cdots (n_i - 1)\theta_{NH_3,i}\right]^{\neq} \overset{\nu_i^{\neq}}{\rightarrow} \rightarrow (n_i - 1)\theta_{NH_3,i} + \theta_i + NH_3 \uparrow, \quad (5)$$

One can find a similar description of the process in a number of works, where an equilibrium distribution strongly shifted toward the reactants is assumed between the reactants and the activated state [24]. Simulation of the desorption process sometimes assume that the adsorbed molecule in the activated state possesses properties similar to the gaseous state. Such an assumption can indeed be used in the Langmuir modeling of physical adsorption, where the activation energy is exactly the same as the enthalpy of desorption. In this case, an equilibrium between the activated state and the reactants is considered as between a gas and an adsorbed molecule under some additional conditions, viz. the adsorbed gas is a lattice gas and cannot possess all translational degrees of freedom (0 to 2 degrees are conserved depending on the binding energy of the molecule to the surface) [25], and the rotational degrees of freedom in the activated state are fully conserved as for a gas and represent a kind of "spinning top" [26] while vibrational degrees of freedom are fully taken into account. Most often, the theory of the activated state in this form is used to estimate the pre-exponential multiplier to simplify calculations and the search for the observed reaction order (the activation energy is determined by the Friedman method conventional for thermal analysis) [27].

In this work, we do not use the activated complex theory; rather, we rely on the Polanyi-Wigner equation to determine the kinetic parameters by mathematical processing methods primarily based on the following assumptions. The degree of surface filling for the *i*th centers is directly related to their total acidity, which is a constant value during adsorption and desorption, so the equations hold

$$\begin{cases} h_i = -\dfrac{dH_i}{dT} = \dfrac{k_0,i}{\beta}\exp\left(-\dfrac{E_{D,i}}{RT}\right)H_i^n, \\ h_i = -H_{\max,i}\dfrac{d\theta_{NH_3,i}}{dT}, \\ H_i = H_{\max,i}\cdot\theta_{NH_3,i}, \\ \theta_{NH_3,i} + \theta_i = 1, \\ h_{cat} = \sum_{i=1}^{n} h_i, \\ H_{cat} = \sum_{i=1}^{n} H_{\max.i}, \end{cases} \quad (6)$$

where h_t is the differential acidity of the *i*th center equaling the rate of ammonia release from the catalyst surface, H_t is the integral acidity equaling the residual concentration of ammonia on the catalyst surface, $H_{max,i}$ is the total acidity of the *i*th centers of ammonia adsorption equaling their initial concentration before desorption, h_{cat} is the rate of ammonia release from all centers at the given instant and temperature — it is this value that is most often presented as the result of NH_3 TPD, H_{cat} is the total acidity value representing the concentration of all adsorption centers on the studied catalyst, and $k_{0,i}$ is the Arrhenius pre-exponential multiplier, the dimensionality of which depends on the observed reaction order. The kinetic model consisting of Eqs. (4)–(6) and proposed in [19] describes the desorption process, but one should take into account that the desorption reactions should be simple and have an activation barrier, i.e., unlike the model in [19], which took the orders to be n = 0, 1, 2. In our proposed model, the orders should be only integer in the subsequent range of values n = 1, 2, 3 as well, which correlates with the criteria presented in the works of S. Vyazovkin [28]. In this case, the role of neighboring adsorbed ammonia molecules in such a model of the desorption process can be associated with filling the lack of

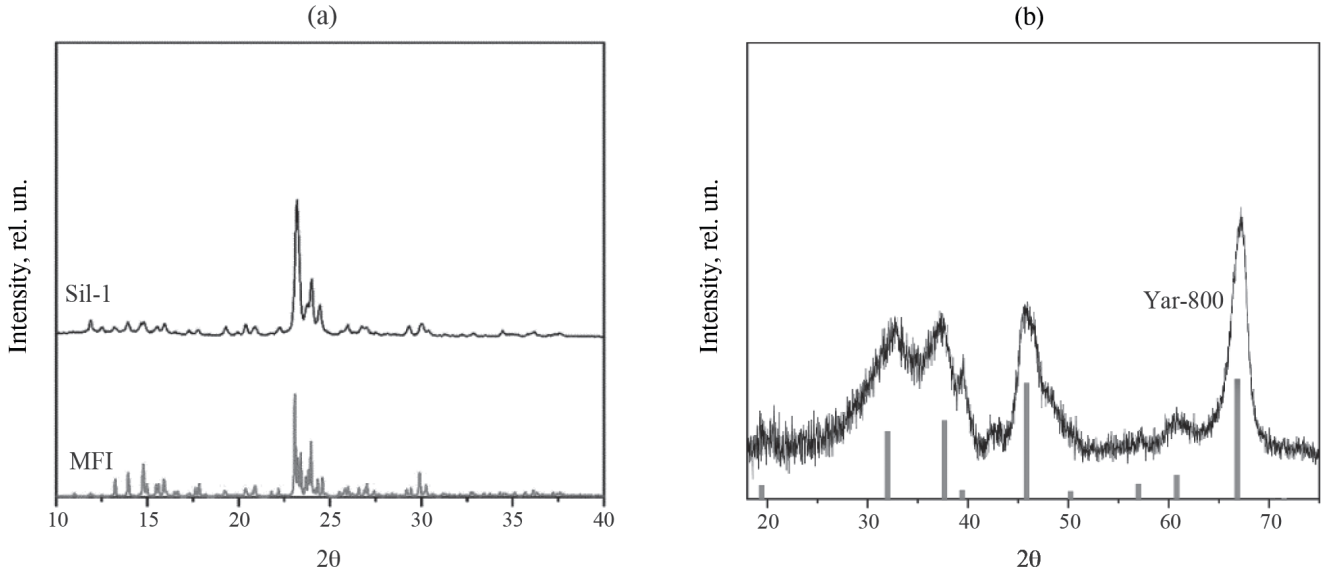

Fig. 2. Diffractograms of the studied samples: silicalite-1 (Sil-1) (a) and aluminum oxide (Yar-800) (b). Comparison data (blue) are taken from COD for zeolite of the MFI structural type and ICDD PDF-2 for γ-Al_2O_3.

energy spent to overcome the activation barrier of the process.

It is these points that we proceed from when describing the process of ammonia desorption from the catalyst surface. This work presents an algorithm for selecting parameters of the equations of kinetic curves according to (4)–(6) and demonstrates the possibilities of the proposed approach for obtaining quantitative characteristics of the surface acidity of a number of materials.

EXPERIMENTAL PART

Systems under Study

For the study, we chose the materials widely used as carriers and catalysts — (1) zeolites with the structural MFI type, for which the ammonia desorption curve has one peak, with different chemical composition, and (2) a number of samples based on γ-Al_2O_3 with a more complex desorption curve obtained from different precursors. Phase-pure silicalite-1 (Sil-1) previously prepared and presented in [29], as well as titansilicalite-1 (TS-1) ZD-07031 produced by Zeolyst International (Germany), were referred to the first type. To study the kinetics of ammonia desorption, three samples of γ-Al_2O_3 were chosen as alumina-oxide systems, viz. (1) industrial granular mesoporous γ-Al_2O_3 prepared out of pseudoboehmite produced by Altayluminofor (Russia) using the technique of extrusion of plastic mass containing 30 wt% of polymer template for macropore formation, followed by calcination at temperatures of 700 and 800°C (Yar-700 and Yar-800 samples, respectively) similarly to the methods given in [31, 32]. All samples were characterized using X-ray diffraction techniques and have confirmed structure (Fig. 2). The properties of the porous structure were calculated using the low-temperature nitrogen adsorption-desorption isotherms of the samples prepared on an Autosorb 6B-KR (Quantachrome, USA). The sample was preliminary degassed at 150°C for 3 h. The specific surface area was calculated using the Brunauer-Emmett-Teller (BET) equation, and the pore volume was calculated using the adsorption value at the maximum achieved pressure. The elemental composition of the samples was determined by atomic emission spectrometry with excitation in inductively coupled plasma (ICP-AES) on an iCAP 6500 Duo spectrometer (ThermoElemental, USA). Table 1 gives the physicochemical characteristics of the studied materials.

The granular materials were ground to a fraction of 0.2–0.8 mm to reduce the influence of diffusion prior to TPD measurement.

Methodology of the Experiment

Temperature-programmed desorption of ammonia was carried out in a quartz reactor with an inner diameter of ∅ 8 mm. For qualitative analysis, a 200–700 mg portion of the analyzed sample was used to obtain reliable desorption data, in which the contribution of diffusion and heat transfer effects is negligible. The sample was ground and sieved to a

Table 1. Physicochemical properties of the studied samples

Sample	S_{sp}, m^2/g	V_{por}, ml/g	Elemental composition
ZD-03071	508	0.82	1.9 wt% Ti 75 wt% Si
Sil^{-1}	414	0.89	47 wt% Si
A1	240	0.59	51–53 wt% Al[a]
Yar-700	186	0.60	
Yar-800	157	0.63	

Remark. [a]For metastable aluminum oxides, losses on ignition above 700°C are less than the relative error of determining the elemental composition by ICP-AES method; S_{sp} is the specific surface area, and V_{por} is the pore volume.

fraction of 0.2–0.8 mm before measurement, then poured into the reactor. The temperature was recorded with a thermocouple placed in the sample layer. During the whole experiment helium (produced by Orenburg Helium Plant, a branch of Gazprom Pererabotka) was passed through the reactor at a constant rate of ~60 ml/min. The experiment was conducted in several stages:

(1) Training of the sample in the helium flow. This was carried out to primarily remove adsorbed water from the surface. At this stage, the reactor was heated to a temperature of 600°C at a rate of 600 K/h, then kept at a constant temperature for another 30 minutes. The reactor was then cooled to a temperature of 100°C.

(2) Saturating the sample with ammonia (Chistye Gazy Plyus, Novosibirsk). For this purpose, ammonia pre-dried over reactivated in NaOH (produced by Khimprom, Novocheboksarsk) carbon AGM-1 (produced by Sorbent, Perm) was fed at a rate of 30 ml/min into a helium stream of 60 ml/min for 30 min until complete saturation of the analyzed sample with ammonia, which was checked using an RGA100 mass spectrometer (produced by Stanford Research System) by the output curve. Then, the ammonia supply was stopped and the reactor was purged with pure helium at a fixed temperature 100°C for another 30 min to remove residual gaseous and physically adsorbed ammonia from the surface of the analyzed catalyst.

(3) Ammonia desorption. This step was carried out at an approximately constant heating rate of ~600 K/h in the helium flow of ~60 mL/min. At the reactor outlet, a portion of the flow was sampled for quantitative analysis of the separated ammonia using a mass spectrometer.

Ammonia signal registration was carried out simultaneously with helium signal registration at the following ionizer settings: 24 V, 10 W. The pressure in the measuring chamber during the experiment was set to 10^{-5} mbar by adjusting the inlet valve gate. For the TPD NH_3 analysis, we used two registration signals (4 a.m.u. for helium and 17 a.m.u. for ammonia), carrying out imaging in the range of signal linearity (the ammonia signal intensity does not exceed 10% threshold of the helium signal intensity). After imaging, the resulting mass spectrometer signal was first synchronized on a time scale with the temperature signal, taking into account the dead volume and the delay in the onset of heating after start-up. Then, using pre-calibrated values of the detector sensitivity factor to ammonia in the helium-ammonia mixture $f_{NH_3} = 0.2055$, the signals were converted to the recorded ammonia release rate, assuming the gases to be ideal, by the formula

$$\overline{n_{NH_3}}\left[\text{mol}/(\text{sg})\right] = \frac{f_{NH_3} \cdot F_{NH_3}}{F_{He}} U_{He} \cdot \frac{p_0}{RT \cdot m_{sample}}, \qquad (7)$$

where p_0 is the atmospheric pressure (Pa), T is the temperature (K), R is the universal gas constant (J/(mol K)), U_{He} is the helium volumetric flow rate (m^3/s), F_{He} are the registered signals of ammonia and helium at the current instant, respectively, F_{NH_3} is the sensitivity factor of the detector to ammonia in helium, and m_{sample} is the sample mass (g).

Using the obtained ammonia release rate, the specific acidity of the sample surface was obtained by the equation

$$h_{cat}\left[\text{mmol}/(\text{Kml})\right] = \overline{n_{NH_3}} \cdot \frac{\rho}{\beta}, \qquad (8)$$

where ρ is the bulk density of the sample (g/ml), β is the heating rate (K/s)

The obtained dependence of the value of specific acidity $h_{cat}(T)$ on temperature was used for mathematical modeling of NH_3 desorption kinetics.

Ammonia TPD curves shown in Fig. 3 were obtained for all analyzed samples. Table 2 gives the conditions for registration and desorption process as well as physical characteristics for each sample.

Parameter Selection

As we can see from system (6) and Eq. (4), there is a relationship between the kinetic pre-exponential

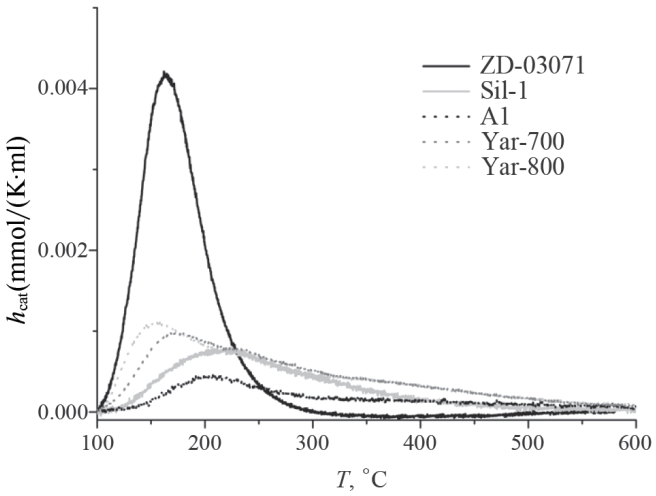

Fig. 3. Ammonia TPD curves of the tested samples.

Table 2. Ammonia TPD conditions for the samples involved.

Sample	U_{He}, cm^3/min	β, K/h	m_{sample}, mg	ρ, g/cm^3
ZD-03071	59.4	638	803.45	0.98
Sil-1	60.7	598	360.00	1.00
A1	59.1	753	544.26	0.96
Yar-700	58.3	639	530.86	0.94
Yar-800	61.0	646	641.17	0.96

Designations. U_{He} is the helium volumetric flow rate, β is the heating rate, m is the sample mass, and ρ is the bulk density.

multiplier $k_{0,i}$ ($M^{(1-n)}c^{-1}$) and the reduced oscillation frequency along the desorption reaction coordinate ν_i (1/K)

$$k_{0,i} = \beta \cdot \nu_i \cdot H_{\max,i}^{(1-n)} \quad (9)$$

Using (9), we can solve the stated problem of fitting the parameters of Eq. (4) ν_i, n, $E_{D,i}$ by the nonlinear minimization method and find $\theta_{NH_3,i}(T)$. Using $\theta_{NH_3,i}(T)$, we can also estimate $\frac{d\theta_{NH_3,i}}{dT}(T)$, which is directly related to the temperature dependence of differential acidity of the ith adsorption centers $h_i(T)$ by the first equation of the system

$$\begin{cases} h_i = -H_{\max,i}\dfrac{d\theta_{NH_3,i}}{dT} \\ h_{cat}(T) = \sum_i h_i. \end{cases} \quad (10)$$

The sum of the differential acidities across all centers yields the differential acidity h_{cat} for the sample (the second equation of the system (10)).

This simulation was performed for a specific type of acid centers using a Mathlab script by the algorithm for solving differential equations by the Runge-Kutta method [33, 34]

*[t,y] = ode45(@(t,y) (-v)*exp(-Ed/8.314/t)*(y).^n, [Tmin:dT:Tmax], y_0); %Diff. equation*

dtetha = –diff(y); %Calculating the derivative function to estimate the desorption rate

m = (Tmax-Tmin)/dT; %Calculating the number of output points for each data set

for l = [1:m]; %Cycle to form output arrays

T(l) = t(l)-273.15; %Temperature conversion from Kelvin to Celsius degrees

*Hi(l) = Hmax*y(l); %Calculating the integral acidity of the ith center at the point T(l)*

*hi(l) = Hmax*dtheta(l); %Calculating the desorption rate at the point T(l)*

end; %Logical end of the script

As input calculation parameters, we used *Tmin*, *dT*, *Tmax,* which are the initial temperature, the temperature step, and the final temperature in K; *Hmax*, which is the maximum concentration of the *i*th acidity center in mol/L; *v*, which is the reduced frequency of oscillation along the desorption coordinate in 1/K; *Ed*, which is the desorption activation energy in J/mol; *n*, which is the observed order of ammonia desorption; and y_0, which is the initial value of degree of ammonia filling of the surface equaling 1. As output data, we obtained arrays of the concentration of the remaining ammonia-filled centers *Hi(l)* (mol/L), the differential acidity $h_i(l)$ (mmol/(K mL)) of the *i*th acid centers, and the temperatures corresponding to these points in °C. This script can be integrated with most programming languages to solve the problem of describing the kinetic curves, selecting parameters $\nu_i, E_{D,i}, n_i, H_{\max,i}$ for each type of centers by a variative method, obtaining a set of arrays $h_i(T)$ as the output, the sum of which for the same temperatures should correspond to the experimental value of acidity.

Analyzing the Influence of Kinetic Parameters on Model Curves

To substantiate the approach to selecting parameters of the kinetic system, we analyze their influence on the shape of the model curve.

First of all, we should emphasize the influence of the observed reaction order (Fig. 4a). One can see that

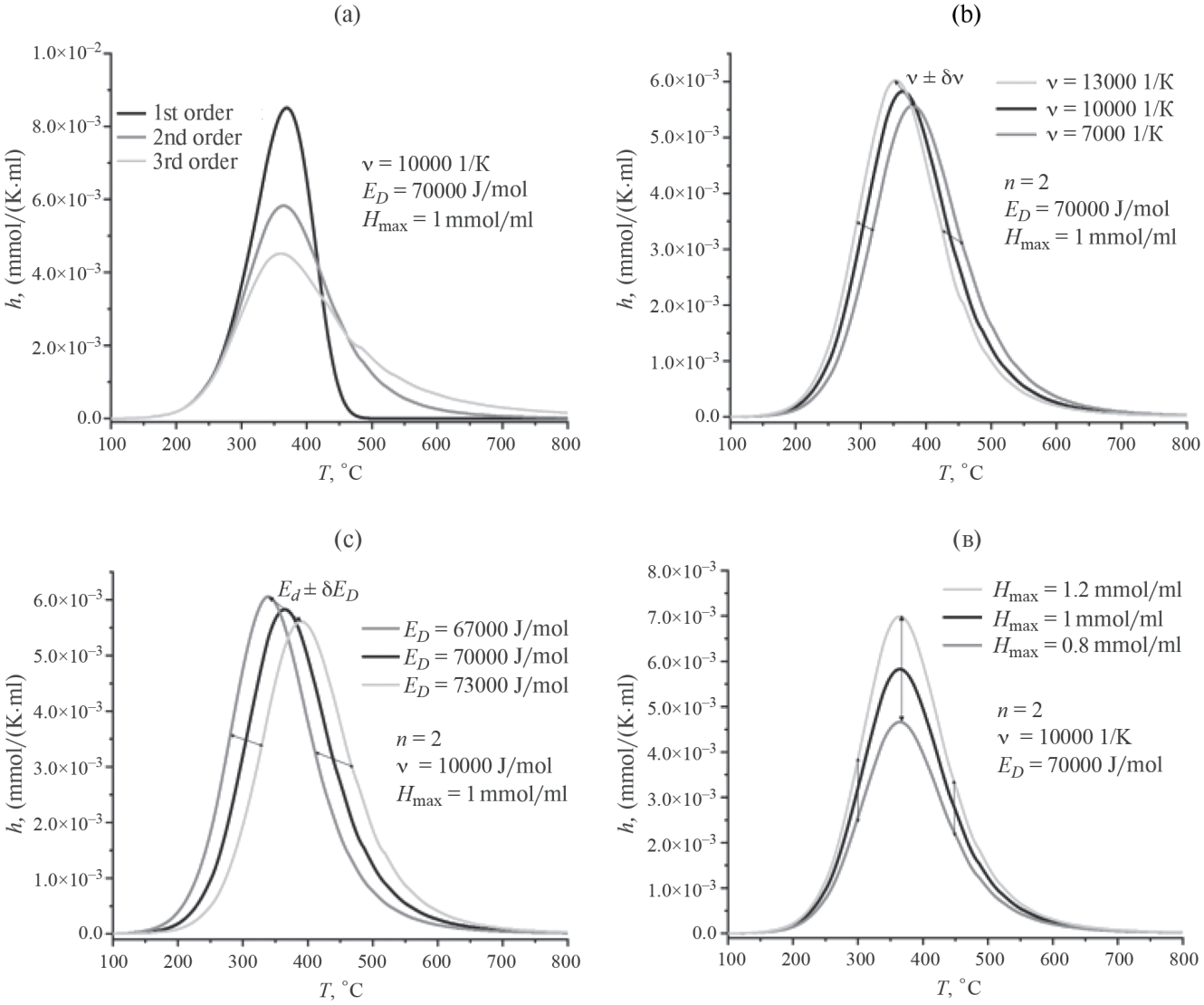

Fig. 4. Effect of different parameters of the kinetic equation on the general shape of the kinetic curve — observed order (a); pre-exponential multiplier (of the reduced frequency along the desorption coordinate) (b); desorption activation energy (c); and integral acidity (d).

a change in the reaction order affects the ratio of the left (rising) and right (descending) branches of the desorption peaks (curves to the left and right of the maximum). For the first order, the left branch is more flattened than the right branch, which has a drastic drop after the maximum ammonia release rate is reached. In addition, for the same values of other parameters, the first order is characterized by a higher value of the differential acidity maximum.

The second order of desorption is characterized by a more symmetric shape of the kinetic curve; one can even assume that the second order desorption should be described by a Gaussian distribution, but there is a broadening of the peak in the high-temperature region associated with the slowing down of the reaction due to a drop in the concentration of acid centers filled with ammonia. The third order of desorption has a more sharply growing left branch and a relatively elongated right branch.

It is worth stipulating in advance that since we assumed that the desorption process is a simple reaction, the orders can only be integer, and therefore we will select them based on the general appearance of the curves and the relation between the experimental branches of the peaks. This approach should reduce the time for parameter selection by a factor of 3^m, where m is the number of the peaks analyzed, since we will not perform the variation of the reaction orders. For other parameters, the situation is simpler since a change in their δ neighborhood does not globally change the curve

shape and only predictably affects the position or height of the peak.

A change in the oscillation frequency along the reaction coordinate leads to a shift of the peak to a lower temperature region with an increase in the peak height and a decrease in its width (Fig. 4b). For the activation energy, we have the opposite effect, viz. the increase in the energy barrier shifts the peak position to the high-temperature region with the peak height decreased and the peak broadened (Fig. 4c). The increasing the concentration of adsorbed ammonia affects only the area and height of the peak, leaving the position of its maximum unchanged (Fig. 4d).

Database of TPD Kinetic Curves

We proceed to the method of selecting kinetic parameters. After the ammonia desorption curve is obtained, it is necessary first to initialize the parameters of the model, which, in turn, requires a database. Therefore, a database of values of kinetic parameters and respective output points in the coordinates $h_i(T)$ with step 1°C and integral acidity H_{max} = 1 mmol/ml was preliminarily created. Each array of such data contains 1,000 points for a particular set of parameters. At the time of preparation of this work, the database contained 260 curves, where the points were fitted for various values of n = 1, 2, 3, ν from 2 to 10^{15} 1/K (with a step multiplier), and E_D from 20 to 170 kJ/mol (with a random step). In this case, most of the curves corresponded to the output of the maximum desorption rate at temperatures of 100–800°C, and for each value of one parameter, the table contained more than a dozen kinetic data sets with other parameters varied over a wide range, leaving only H_{max} constant. The database is periodically supplemented with new experimental values of parameters and their respective kinetic curve points.

Note also that the temperature step dT will not always give values coinciding with the experimental one. Therefore, at each iteration of parameter selection, it was necessary to interpolate the model points to the experimental points to adequately estimate the determination coefficient. In this work, linear interpolation was used because of the small temperature step in modeling the desorption process (0.1°C).

Initialization Algorithm for Initial Parameters for Experimental TPD Curves

The parameter initialization for the experimental values h(T) was carried out by peak positions to estimate the observed order, activation energy, pre-exponential multiplier, and integral acidity of the centers using the following algorithm.

(1) Determine the maximum value h_{max} from the graph.

(2) In the ε-neighborhood from the peak maximum, which is defined by the set of peak points from $0.5h_{max}$ of the left branch to $0.8h_{max}$ of the right branch, all experimental points are selected and then compared with previously analyzed ammonia desorption curves with the known parameters and standard acidity H_{max} = 1 mmol/ml from the database. Curves with the position of the maximum value of the desorption rate h differing from the experimental one by more than 10°C are not considered. The rest of parameters are checked for additional conditions of compliance with the experimental curve.

(3) In the range of points from $0.5h_{max}$ of the left branch to $0.8h_{max}$ of the right branch, the temperature range is determined, over which the integrals for the tabular and experimental curves are calculated. Their ratio is used to determine the valueH_{max} for the tabular curve, which is used in further calculations (Fig. 5a).

(4) Further, for each initialized model curve in the given temperature range, the determination coefficient R^2 is calculated using the following algorithm

$$\begin{cases} \bar{h} = \dfrac{1}{n}\sum\limits_{j}^{n} h_j, \\ \sigma_h^2 = \sum\limits_{j}^{n} (h_j - \bar{h})^2 \\ \sigma^2 = \sum\limits_{j}^{n} (h_j - h(T_j))^2, \\ R^2 = 1 - \dfrac{\sigma^2}{\sigma_h^2}, \end{cases} \tag{11}$$

where h_j is the experimentally obtained value of acidity at temperature T_j, $h(T_j)$ is the model value calculated for T_j, and h is the average value of the experimentally measured value for the entire recorded value of the desorption rate. For the experimental peak, the set of tabulated parameters that provides the highest determination coefficient is selected, as shown in Fig. 5b.

(5) If $R^2 > 0.95$ for the entire TPD curve, the program automatically suggests using these parameters in further selection, and this completes the

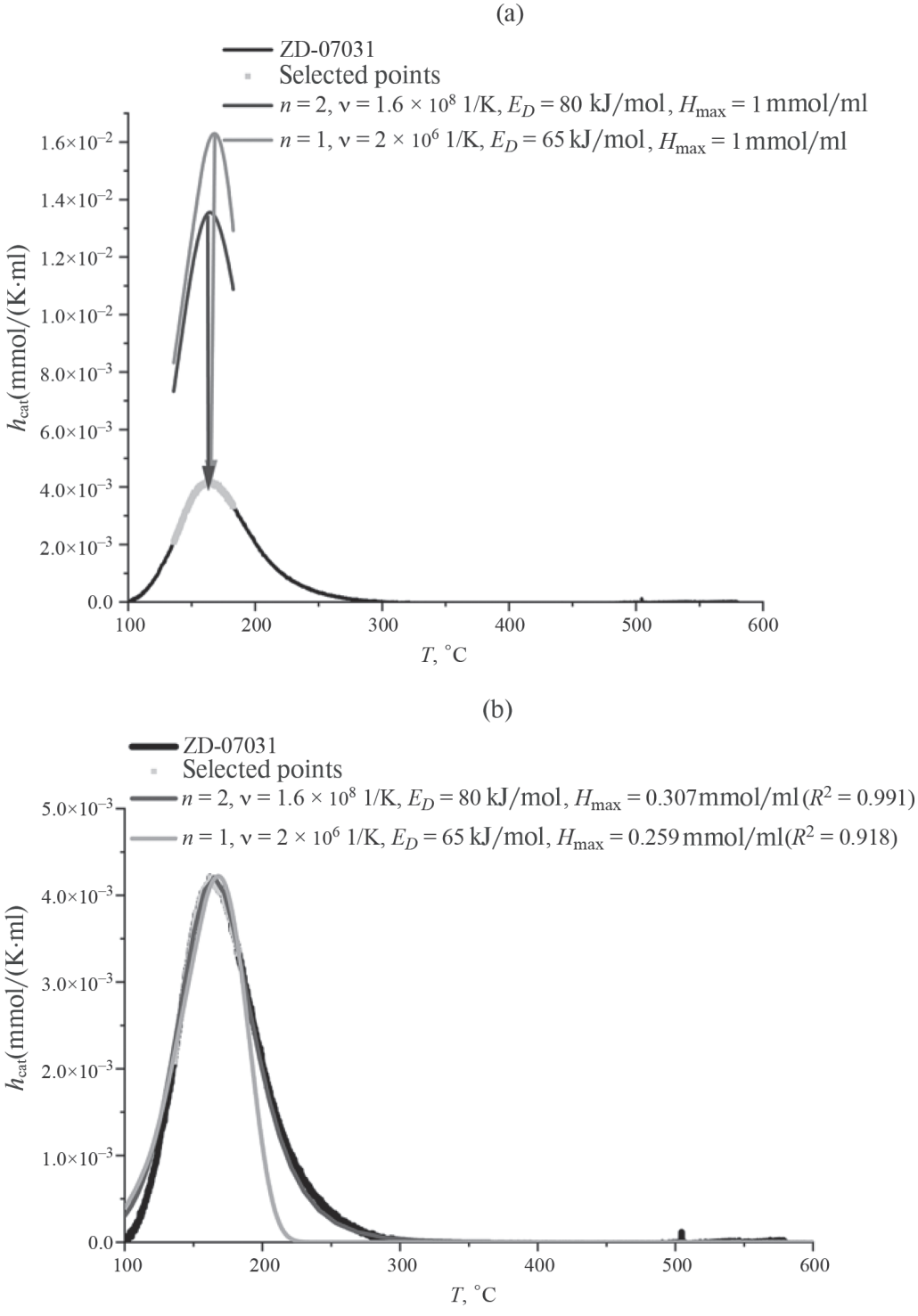

Fig. 5. Initialization of parameters from the database, where the section of kinetic curves that best fits the maximum desorption rate is selected (a), and afterwards the curve with the highest determination coefficient (blue line) is chosen (b).

initialization. Thus, for instance, Fig. 5 shows a variant of the automated initialization of parameters for the TPD result when analyzing the commercial sample ZD-07031 (titansilicalite-1) such that $R^2 = 0.991$ for its selected parameters.

(6) If the determination coefficient turned to be less than 0.95, the difference with the selected model is calculated for the experimental points and steps 1–6 are repeated to initialize the next set of parameters from the database and select the most suitable one.

(7) The initialization procedure ends when three TPD kinetic curves are selected or lasts until the determination coefficient is greater than 0.95. At the same time, the user always can manually adjust the initialized data with the output of the result in the form of the curve $h(T)$ and the determination coefficient for experimental and model points. For instance, Fig. 6 shows the initialization of parameters for the Yar-800 aluminum oxide sample. Each model curve was initialized sequentially by the difference with experimentally obtained points.

Algorithm for Optimizing Simulation Parameters to Improve Convergence with Experimental Results

The process was carried out in a cycle with construction of model curves of the ammonia desorption rate, in which the parameters were varied within the deviation from their values at the current iteration step. In this case, the deviation for each parameter was chosen dynamically, based on the error of the TPD model at the current step. The iteration error was estimated based on the coefficient of determination by the formula

$$Error = \sqrt{\left(1 - R^2\right)} \qquad (12)$$

The value found was used to estimate the individual parameter deviations in the optimization cycle by the formulas

$$\begin{cases} d\nu_i = Error \cdot rate_{\nu_i} \cdot \nu_i, \\ dH_{\max,i} = Error \cdot rate_{H_{\max,i}} \cdot H_{\max,i}, \\ dE_{D,i} = Error \cdot rate_{E_{D,i}} \cdot 5180, \end{cases} \qquad (13)$$

where $d\nu_i$ is the deviation from the current value ν_i, $dH_{\max,i}$ is the deviation from the current value $H_{\max,i}$, $dE_{D,i}$ is the deviation from the current value of ammonia desorption activation energy, $rate_{x_i}$ are the individual selection rates of the model parameters for the parameter x_i, which are numerically taken equal to one before the first iteration. One can see that all deviations except the deviation of the desorption activation energy depend directly on the current values of the parameters themselves. However, because of its significant influence on the desorption rate of ammonia (the energy is in the exponential part of the formula), this approach for the desorption activation energy does not allow us to set the deviation to be linearly dependent on the current value $E_{D,i}$. The value corresponding to the average value RT, i.e., at temperature 350°C, equaling 5180 J/mol, was chosen as the standard value for calculating the energy deviation.

The rates of change $rate_{x_i}$ are not constant for several reasons, viz. (1) an excessively big rate of change in the parameter near its optimum value will not allow the optimum to be reached, and (2) with a constant individual rate of selection away from the optimum value, the change in the parameter will be insufficient to reach the optimum quickly. Therefore, the individual rates $rate_{x_i}$ were also varied depending on how the parameter x_i of the model changed by the following algorithm

$$rate_{n+1,x_i} = \begin{cases} 0.9 \cdot rate_{n,x_i}, \text{если } x_{n+1,i} = x_{n,i} \\ rate_{n,x_i}, \text{если } x_{n+1,i} = x_{n,i} \pm dx_{n,i} \text{ первый раз} \\ 1.1 \cdot rate_{n,x_i}, \text{если } x_{n+1,i} = x_{n,i} \pm dx_{n,i} \\ \text{более раз}, \end{cases}, \qquad (14)$$

where the index m is the number of the current parameter selection iteration. Thus, if the parameter in simulation is actively changing, the rate of its change increases; otherwise, on the contrary, there is a decrease in the rate of selection for more accurate optimization of the parameter, viz. increasing the determination coefficient.

In this case, all possible variants are searched through in each cycle of parameter selection. For instance, to describe a kinetic curve with two equations, all parameters for two curves are simultaneously searched through

$$\left\{\nu_1 - d\nu_1;\ \nu_1;\ \nu_1 + d\nu_1\right\},$$
$$\left\{E_{D,1} - dE_{D,1}; E_{D,1}; E_{D,1} + dE_{D,1}\right\},$$
$$\left\{H_{\max,1} - dH_{\max,1};\ H_{\max,1}; H_{\max,1} + H_{\max,1}\right\},$$
$$\left\{\nu_2 - d\nu_2;\ \nu_2;\ \nu_2 + d\nu_2\right\},$$
$$\left\{E_{D,2} - dE_{D,2}; E_{D,2}; E_{D,2} + dE_{D,2}\right\},$$
$$\left\{H_{\max,2} - dH_{\max,2};\ H_{\max,2}; H_{\max,2} + dH_{\max,2}\right\}.$$

The experimental points are compared to each of the obtained variants of the kinetic curves and R^2 is determined for each of them. The obtained values of the determination coefficient are compared to each other to determine one most appropriate set of parameters out of $3^6 = 729$. It is on this set that the individual parameter selection rate is recalculated, and the optimization procedure is repeated at the next step according to Eq. (14).

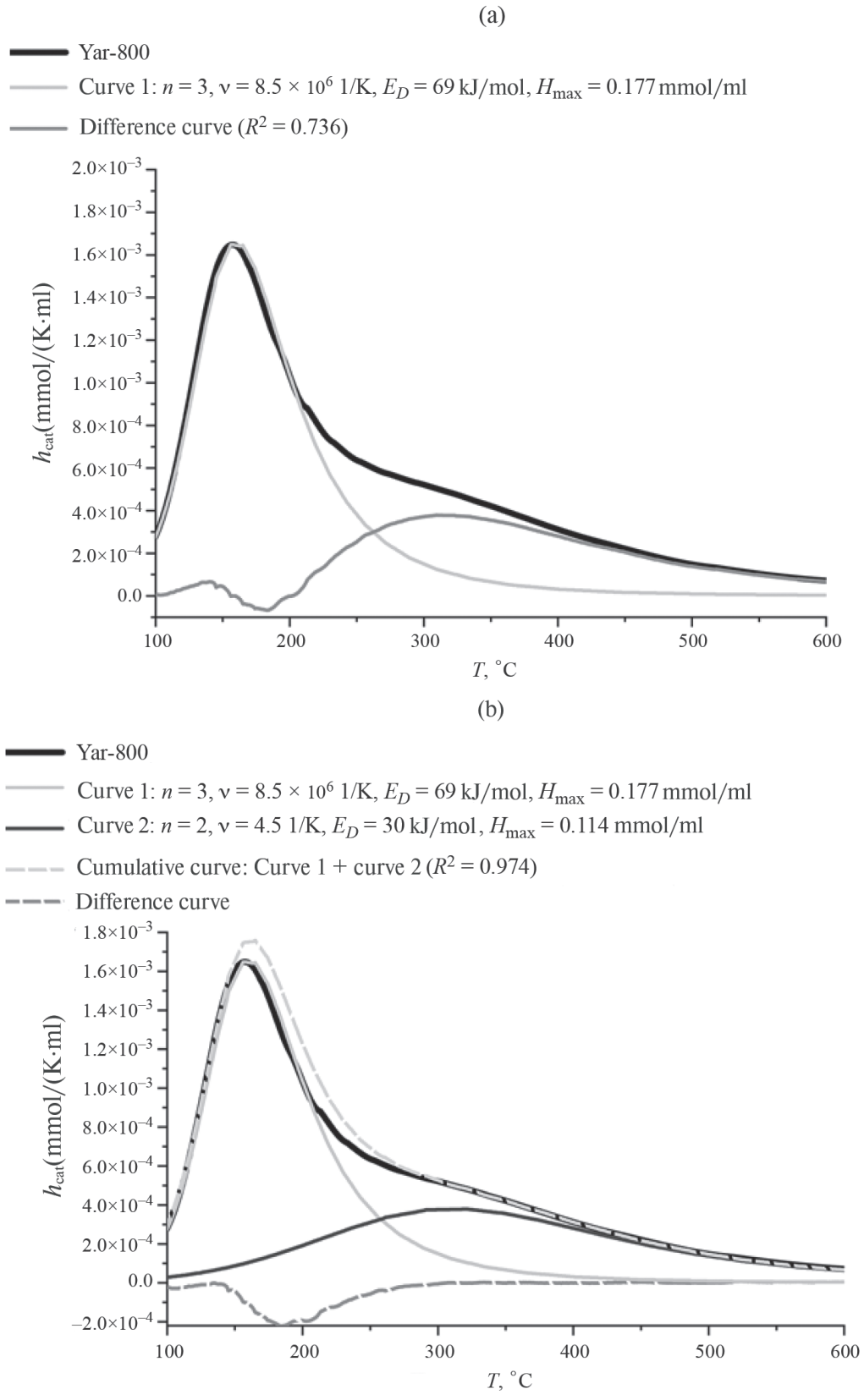

Fig. 6. Initialization of kinetic parameters for the TPD curve of g-aluminum oxide Yar-800, selection of the parameters of the first curve from the database, checking the convergence of the model (a) and adding an additional kinetic curve due to the low R2 value after substituting the first curve (b).

Parameter selection is finished if one of two conditions holds, viz. (1) if the determination coefficient obtained for the parameters is $R^2 = 1$, which means that there is no simulation error, and (2) if all parameters stop changing for more than five consecutive iterations with their individual selection rates decreased, where the deviations will be the errors of the obtained model parameters.

DISCUSSION OF RESULTS

The final stage of simulation involves calculating the true kinetic pre-exponents according to formula (9) and outputing all found parameters of the model. The block diagram of the described parameter selection is presented in Fig. 7.

To confirm the applicability of the model, it is necessary to demonstrate that desorption can indeed proceed by a third-order reaction. Moreover, it is desirable to show that the process can be monocentric, i.e., it proceeds by desorption from centers having the same set of energy properties (the same pre-exponents and desorption energies). Zeolite systems turned out to have exactly these properties (Fig. 8). In the course of parameter selection for titansilicalite-1 ZD-07031 and silicalite-1 Sil-1 possessing the same MFI structural type, desorption can be described by a single third-order kinetic curve. The monocenteric model is still to be discussed and will be studied in more detail in future works with zeolite-like materials.

It is noteworthy that despite the same structural type of zeolite-like samples (MFI), the ammonia desorption curves have a different shape. The broader desorption peak for silicalite-1 Sil-1 means weaker binding of ammonia to the surface, which is largely compensated by the variability of ammonia adsorption as most of the adsorption sites are identical, and, therefore, the pre-exponential multiplier, which is responsible to a greater extent for the intrinsic oscillation of molecules at the adsorption site, will also be low. Thus, molecules with weak mobility along the surface will be slowly desorbed because they will be less exposed to collision with each other. Given that the observed order of the desorption process is higher than the first order, this may imply that the collisions necessary for the reactions to proceed should also occur less frequently. Collisions are necessary for adsorbate molecules to exchange energy and accumulate it for detachment from the surface — desorption. This is in agreement with the obtained kinetic values of the parameters given in Table 3. In spite of the fact that the study of acidity for zeolites of MFI type requires more detailed consideration, we can consider that the desorption of ammonia according to the third-order kinetic equations is realized and, moreover, the desorbing molecules in triple collisions try to compensate the deficit of energy required to break the bond with the surface.

The description of the kinetics of ammonia desorption from the surface of γ-Al_2O_3 also appears to be quite interesting. In the proposed series of samples of alumina-oxide carriers, despite the very different type of dependence of ammonia desorption rate on temperature, different heating rates, different values of integral acidity, one can observe after processing the curves by the kinetic model, that the main kinetic parameters of the desorption process have very close values, characterizing the affinity between the analyzed samples, viz. all samples have two characteristic desorption peaks, which have the same observed orders. For the first peak ($n = 3$), the characteristic values of the pre-exponent and activation energy of desorption are of the order of 1×10^9 $M^{-2}s^{-1}$ and 77 kJ/mol; for the second one ($n = 2$), k_0 and E_D are of the order of 4 $M^{-1}s^{-1}$ and 28 kJ/mol, respectively (Fig. 9, Table 4).

At first glance, the obtained data may seem to contradict the thermodynamic principles of reaction flow since for a higher temperature region, according to the simulation results, desorption of ammonia from centers with a lower activation barrier is observed. An explanation for such an effect can be found in [35–37], viz. for the low-temperature peaks for aluminum oxide, desorption is usually attributed to desorption of ammonia from Lewis acid centers [36] while the high-temperature peaks are attributed to desorption from Bronsted centers [38]. During the interaction of ammonia with Lewis centers, the adsorbate molecule is coordinated by both the aluminum atom via an unshared nitrogen electron pair and oxygen via hydrogen (Fig. 10a). It is because of the stronger binding to the surface that more energy is required to overcome the barrier for desorption of ammonia from low temperature centers. It is indicated in [39] that adsorbed molecules on the surface can behave as a two-dimensional gas, diffusing along the surface from one adsorption site to a similar other site. For its realization, a sufficient condition is a smaller value of the diffusion activation energy, which is achieved when the adsorption centers are close enough (in this case, the diffusion activation energy is considered to be less than 30% of the desorption activation energy), which is easily realized for Lewis acid centers (Fig. 10b). Since we have second- and third-order desorption kinetics, the movement of ammonia molecules across the catalyst surface directly promotes their collision and energy accumulation at vibrational and rotational levels of adsorbed molecules, which is necessary for desorption into the gas phase.

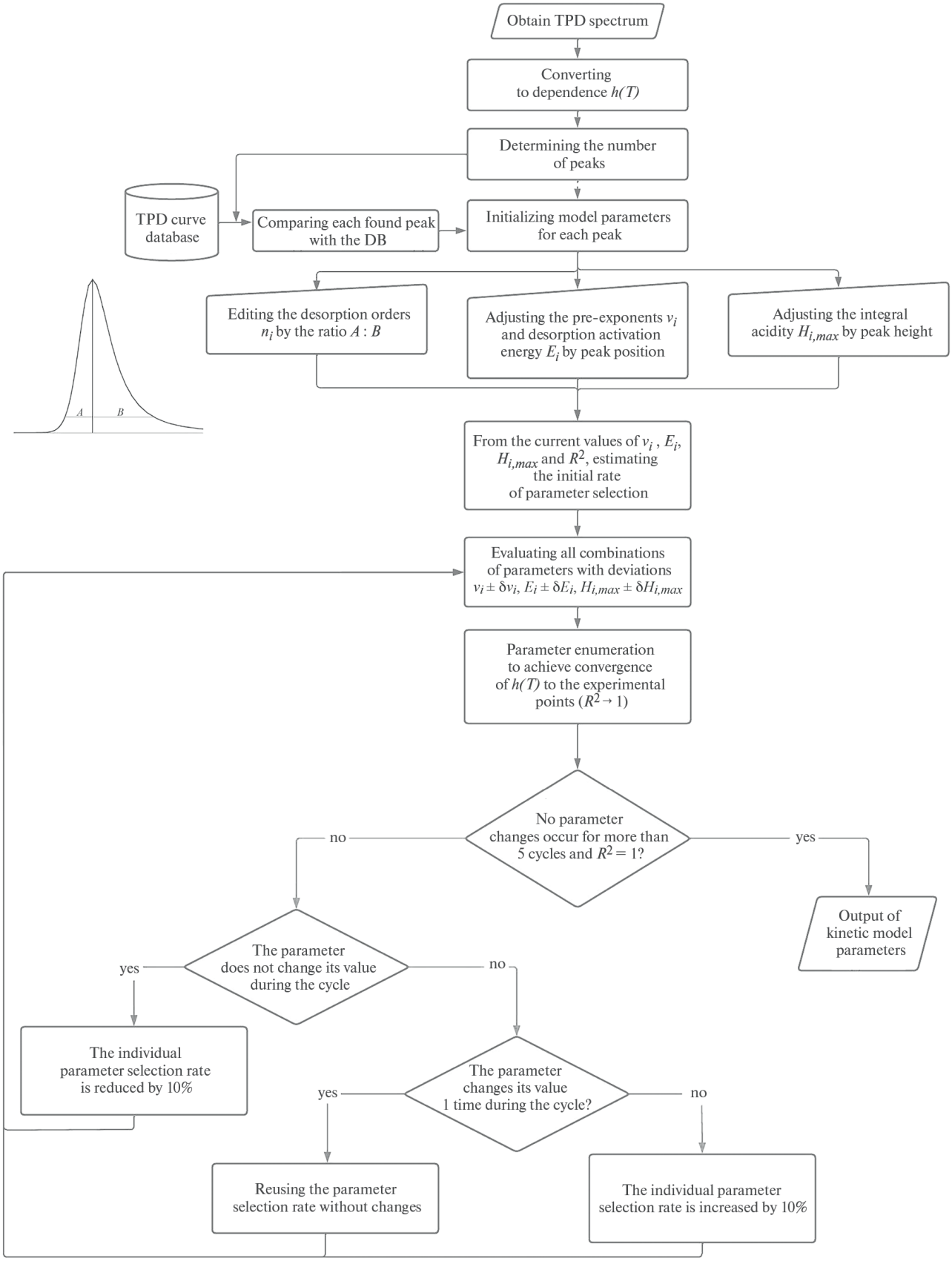

Fig. 7. Block diagram of the algorithm for selecting parameters of the TPD NH_3 kinetic model.

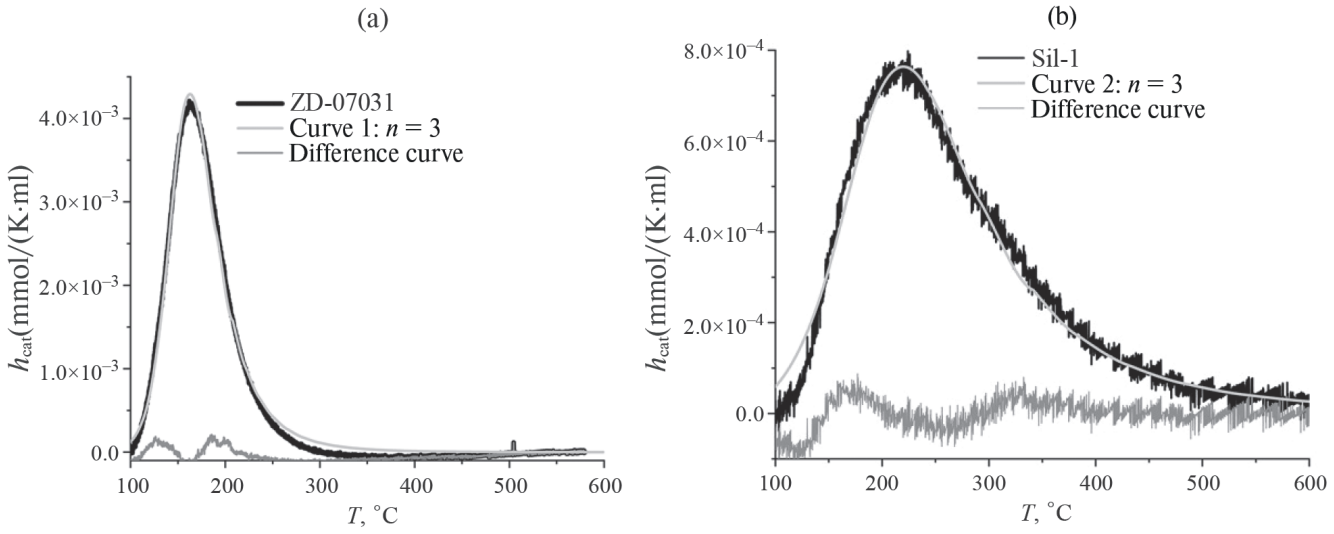

Fig. 8. Ammonia TPD curves for samples ZD-07031 (a) and Sil-1 (b) with deconvolution via the proposed kinetic model.

Table 3. Kinetic parameters of the proposed model for ZD-07031 and Sil-1

Sample	Model parameters					
	n_i	$k_{0,i}$, $M^{(1-n)}$ s^{-1}	$E_{D,i}$, kJ/mol	$H_{max,i}$, M	ν_i, 1/K	R^2
ZD-07031 Curve 1	3	$(897 \pm 2) \times 10^9$	107.6 ± 0.8	0.3090 ± 0.0013	$(484.0 \pm 1.1) \times 10^9$	0.9949
Sil-1 Curve 2	3	23300 ± 270	48.9 ± 0.8	0.1450 ± 0.0008	2960 ± 40	0.9835

For Bronsted acid centers, the situation is opposite: the probability of diffusion of ammonia molecules across the surface is limited due to the much larger distance between them, which prevents vibrational-diffusive motion of molecules along the reaction coordinate and leads to a small value of the pre-exponential multiplier (Fig. 10c, Fig. 10g). Therefore, despite the low activation barrier for desorption, it is more difficult for ammonia located on the Bronsted centers to accumulate the missing energy by finding another molecule to collide with. Apparently, it is this effect that is reflected in the values of the kinetic parameters obtained in the simulations of the ammonia desorption process from the analyzed aluminum oxides. Thus, despite the seeming contradiction of the obtained simulation results to the generally accepted approaches for evaluating the strength of acid centers, the observed ammonia desorption energies from different aluminum oxide centers have a physical sense and, moreover, the obtained values for different samples of the same chemical nature having different integral acidity coincide.

CONCLUSIONS

In this work, we proposed a universal approach for processing the results of temperature-programmed ammonia desorption based on the Polanyi-Wigner kinetic model. One of the important results of modeling the ammonia desorption process is applying the kinetic equation for the third-order reaction rate to describe the experimental ammonia TPD curves. In addition, we proposed an algorithm that allows automatically selecting the parameters of kinetic equations for the obtained experimental dependences of the ammonia desorption rate h_{cat}(mmol/K ml) on the temperature $T(K)$. The proposed algorithm is tested on a number of samples, including zeolite titansilicalite-1 and silicalite-1 systems. Both samples are treated using the third-order single kinetic curve equation with the determination coefficient $R^2 > 0.98$.

According to the proposed methodology, for several different samples of γ-Al_2O_3, we managed to obtain a convergent result by treating the output curves of NH_3 TPD using two kinetic equations with the determination coefficient $R^2 > 0.98$. It was found that the desorption

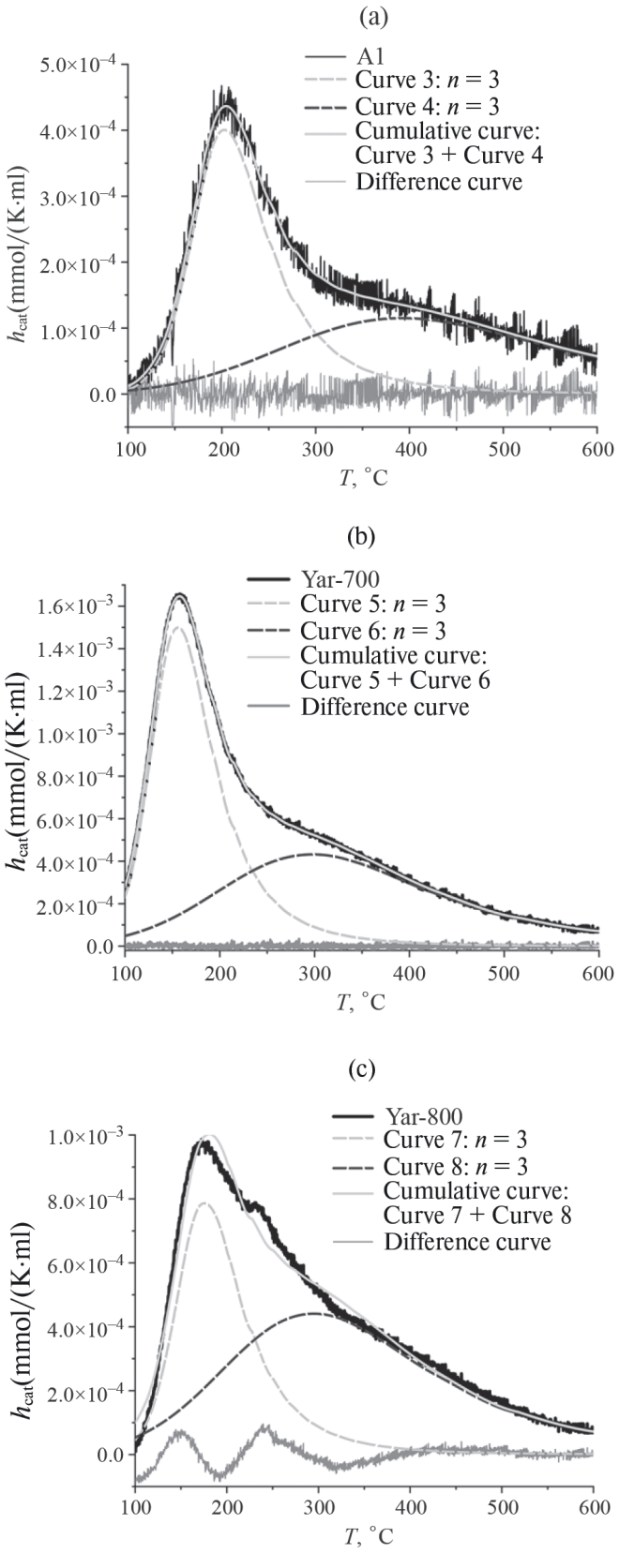

Fig. 9. Ammonia TPD curves of the samples A1 (a), Yar-700 (b), and Yar-800 (c) with deconvolution via the proposed kinetic model.

of ammonia on aluminum oxide could be described by third- and second-order kinetic equations having pre-exponential multipliers and desorption activation energies of 1×10^9 $M^{-2}s^{-1}$ and 77 kJ/mol and 4 $M^{-1}s^{-1}$ and 28 kJ/mol, respectively. Nevertheless, the obtained values of the pre-exponentials differ by ±12% in the series of the studied alumina-oxide systems, which may be related to the model used, where the pre-exponential multipliers in temperature-programmed processes are independent of temperature. In further studies, we will propose ways to process such curves with the mathematical model refined and taking into account the influence of temperature on the pre-exponent.

FUNDING

The work was partially supported by the Ministry of Science and Higher Education of the Russian Federation within the framework of the State Assignment of the Institute of Catalysis SB RAS (project FWUR-2024-0036) for synthetic and experimental work, and young employees were attracted for measurements supported by the grant of the Government of the Novosibirsk region no. gr-10 of September 18, 2023.

CONFLICT OF INTEREST

The authors of this work declare that they have no conflicts of interest.

REFERENCES

1. *Da Ros S., Barbosa-Coutinho E., Schwaab M. et al.* // Mater. Charact. 2013. Vol. 80. P. 50.
2. *Phung T.K., Garbarino G.* // J. Ind. Eng. Chem. 2017. Vol. 47. P. 288.
3. *Yashnik S.A., Boltenkov V. V., Babushkin D.E. et al.* // Kinet. Catal. 2022. Vol. 63. P. 555.
4. *Cvetanovic R.J., Amenomiya Y.* // Adv. Catal. 1972. Vol. 6. P. 21.
5. *Amenomiya Y., Chenier J.H.B., Cvetanović R.J.* // J. Phys. Chem. 1964 Vol. 68. P.52.
6. *Serebrennikov D. V., Grigor'eva N.G., Khazipova A.N. et al.* // Kinet. Catal. 2022. Vol. 63. P. 577.
7. *Wu L., Su H., Liu Q. et al.* // Kinet. Catal. 2022. Vol. 63. P. 498.
8. *Busca G.* // Chem. Rev. 2007. Vol. 107. P. 5366.
9. *Kim C., Yan X.M., White J.M.* // Rev. Sci. Instrum. 2000. Vol. 71. P. 3502.
10. *Kechagiopoulos P.N., Thybaut J.W., Marin G.B.* // Ind. Eng. Chem. 2014. Vol. 53. P. 1825.
11. *Cvetanović R.J., Amenomiya Y.* // Adv. Catal. 1967 Vol. 17. P. 103.

Table 4. Kinetic parameters of the proposed model for A1, Yar-700, and Yar-800

Sample	Model parameters					
	n_i	$k_{0,i}$, $M^{(1-n)}s^{-1}$	$E_{D,i}$, kJ/mol	$H_{max,i}$, M	ν_i, 1/K	R^2
A1 Curve *3* Curve *4*	 3 2	 $(1.067 \pm 0{,}009) \times 10^9$ 4.22 ± 0.04	 77.48 ± 0.03 28.04 ± 0.07	 0.0460 ± 0.0011 0.0480 ± 0.0017	 $(1109 \pm 9) \times 10^4$ 0.967 ± 0.009	0.9846
Yar-700 Curve *5* Curve *6*	3 2	$(0{,}926 \pm 0{,}003) \times 10^9$ 4.37 ± 0.05	77.070 ± 0.016 78.220 ± 0.023	0.1430 ± 0.0015 0.1340 ± 0.0018	$(1062 \pm 4) \times 10^5$ 3.275 ± 0.004	0.9995
Yar-800 Curve *7* Curve *8*	3 2	$(1{,}118 \pm 0{,}003) \times 10^9$ 3.89 ± 0.06	77.590 ± 0.011 27.70 ± 0.06	0.082 ± 0.006 0.138 ± 0.005	$(4198 \pm 4) \times 10^4$ 2.991 ± 0.005	0.9830

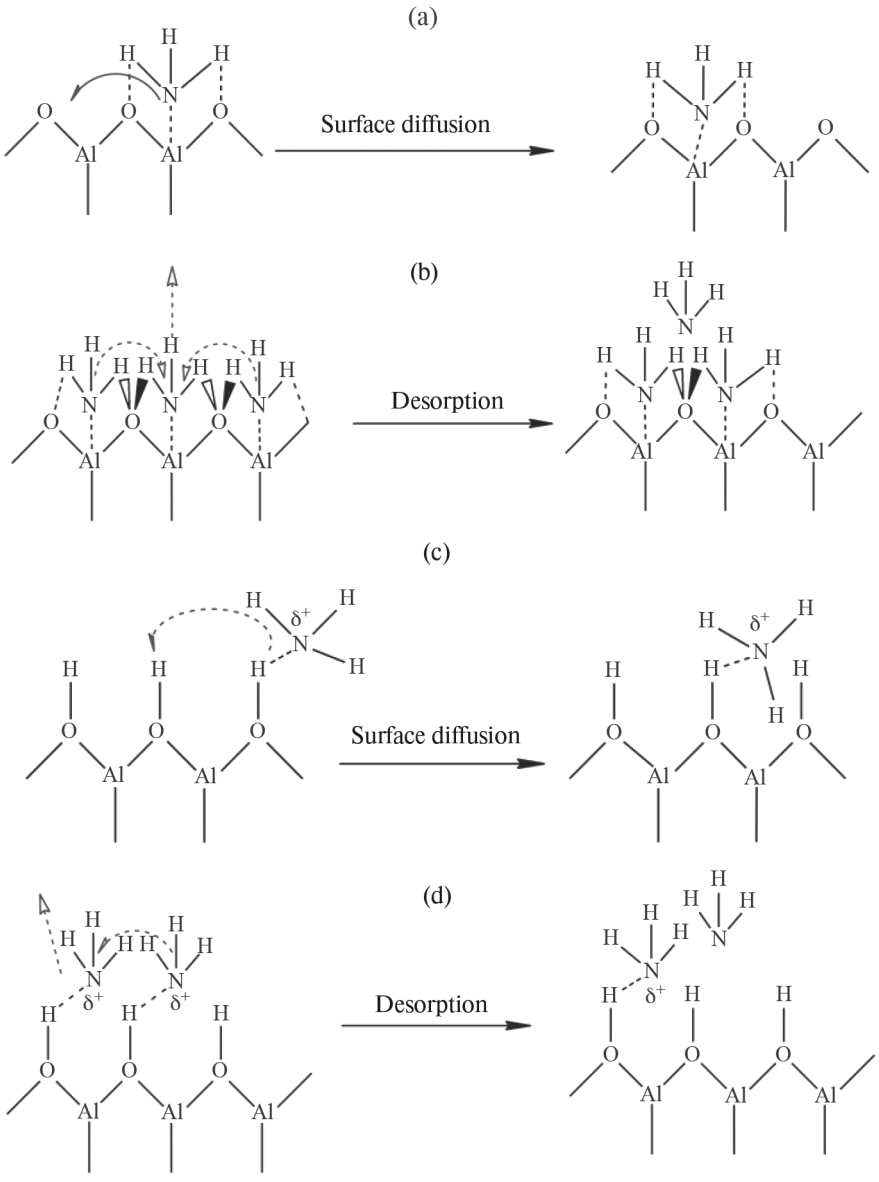

Fig. 10. Peculiarities of surface diffusion of ammonia molecules and their desorption from Lewis (a), (b) and Bronsted (c), (d) acid centers.

12. *Rodríguez-González L., Hermes F., Bertmer M. et al.* // Appl. Catal. A Gen. 2007. Vol. 328. P. 174.
13. *Schwarz J.A.* // Catal. Rev. – Sci. Eng. 1983. Vol. 25. P. 141.
14. *Bhatia S., Beltramini J., Do D.D.* // Catal. Today. 1990. Vol. 7. P. 309.
15. *Kanervo J.M., Krause A.O.I.* // J. Phys. Chem. B. 2001. Vol. 105. P. 9778.
16. *Russell N.M., Ekerdt J.G.* // Surf. Sci. 1996. Vol. 364. Pp. 199–218.
17. *Niwa M., Katada N.* // Chem. Rec. 2013. Vol. 13. P. 432.
18. *Da Ros S., Valter Flores K.A., Schwaab M. et al.* // J. Ind. Eng. Chem. 2021. Vol. 94. P. 425.
19. *Xu J., Deng J.* // ACS Omega. 2020. Vol. 5. P. 4148.
20. *Campbell C.T., Sellers J.R.V.* // Chem. Rev. 2013. Vol. 113. P. 4106.
21. *King D.A.* // Surf. Sci. 1975. Vol. 47. P. 384.
22. *Parmon V.* Thermodynamics of non-equilibrium processes for chemists with a particular application to catalysis // Elsevier. 2010.
23. *Sidoumou M., Panella V., Suzanne J.* // J. Chem. Phys. 1998. Vol. 101. P. 6338.
24. *Schmid M., Parkinson G.S., Diebold U.* // ACS Phys. Chem. Au. 2023. Vol. 3 P. 44.
25. *Sprowl L.H., Campbell C.T., Árnadóttir L.* // J. Phys. Chem. C. 2017. Vol. 121. P. 9655.
26. *Sprowl L.H., Campbell C.T., Árnadóttir L.* // J. Phys. Chem. C. 2016. Vol. 120. P. 9719.
27. *Banerjee A., Vithusha T., Krishna B.B. et al.* // Bioresour. Technol. 2021. Vol. 340 P. 125534.
28. *Vyazovkin S., Burnham A.K., Favergeon L. et al.* // Thermochim. Acta. 2020. Vol. 689. P. 178597.
29. *Luzina E.V., Shamanaeva I.A., Parkhomchuk E.V.* // Pet. Chem. 2021. Vol. 61. P. 807.
30. *Veselovskaya J.V., Parunin P.D., Netskina O.V. et al.* // Energy. 2018. Vol. 159. P. 766.
31. *Semeykina V.S., Polukhin A.V., Lysikov A.I. et al.* // Catal. Letters. 2019. Vol. 3. P. 513.
32. *Parkhomchuk E.V., Fedotov K.V., Lysikov A.I. et al.* // Catal. Ind. 2022. Vol. 14. P. 86.
33. *Dormand J.R., Prince P.J.* // J. Comput. Appl. Math. 1980. Vol. 6. P. 19.
34. *Shampine L.F., Reichelt M.W., Sci S.J.* // Soc. Ind. Appl. Math. 1997. Vol. 18. P. 1.
35. *Lamberov A.A., Khalilov I.F., Ilyasov I.R. et al.* // Vestnik Kazan Tech. Univ. 2011. No. 13. P. 24
36. *Ye Y.L., Fu M.Q., Chen H.L. et al.* // J. Fuel Chem. Technol. 2020 Vol. 48. P. 311.
37. *Efstathiou A.M., Fliatoura K.* // Appl. Catal. B, Environ. 1995. Vol. 6. P. 35.
38. *Guo R., Zhou Y., Pan W. et al.* // J. Ind. Eng. Chem. 2013. Vol. 19. P. 2022.
39. *Zhdanov V.P., Pavlicek J., Knor Z.* // Catal. Rev. – Sci. Eng. 1988. Vol. 30. P. 501.